

Interlayer excitons in bilayer MoS₂ with strong oscillator strength up to room temperature

Iann C. Gerber^{1,*}, Emmanuel Courtade¹, Shivangi Shree¹, Cedric Robert¹, Takashi Taniguchi², Kenji Watanabe², Andrea Balocchi¹, Pierre Renucci¹, Delphine Lagarde¹, Xavier Marie¹, and Bernhard Urbaszek^{1,†}
¹Université de Toulouse, INSA-CNRS-UPS, LPCNO, 135 Av. Rangueil, 31077 Toulouse, France and
²National Institute for Materials Science, Tsukuba, Ibaraki 305-0044, Japan

Coulomb bound electron-hole pairs, excitons, govern the optical properties of semi-conducting transition metal dichalcogenides like MoS₂ and WSe₂. We study optical transitions at the K-point for 2H homobilayer MoS₂ in Density Functional Theory (DFT) including excitonic effects and compare with reflectivity measurements in high quality samples encapsulated in hexagonal BN. In both calculated and measured spectra we find a strong interlayer exciton transition in energy between A and B intralayer excitons, observable for T = 4 – 300 K, whereas no such transition is observed for the monolayer in the same structure in this energy range. The interlayer excitons consist of an electron localized in one layer and a hole state delocalized over the bilayer, which results in the unusual combination of high oscillator strength and a static dipole moment. We also find signatures of interlayer excitons involving the second highest valence band (B) and compare absorption calculations for different bilayer stackings. For homotrilayer MoS₂ we also observe interlayer excitons and an energy splitting between different intralayer A-excitons originating from the middle and outer layers, respectively.

INTRODUCTION

Van der Waals materials have in-plane covalent bonding and the individual layers are held together by the so-called dispersion forces [1, 2]. A fascinating aspect of this class of materials is the drastic change of physical properties by changing the sample thickness by just one atomic monolayer. A prominent example is the striking difference between mono- and bilayer graphene [3]. For the van der Waals semiconductor MoS₂ the transition from indirect to direct bandgap material occurs when going from bilayers to a monolayer [4, 5]. These dramatic changes are very different from classical semiconductors like GaAs for example, where the optical properties change gradually with thickness [6].

The light-matter interaction in monolayer (ML) transition-metal dichalcogenides (TMDs) is governed by Coulomb bound electron-hole pairs, excitons [7–9]. As a second layer is added, the light matter interaction is strongly modified since new exciton complexes can form, with electron and hole residing in different layers [10–14], as sketched in Fig. 1. These interlayer excitons show interesting properties [15], also for thicker layers [16, 17] and more sophisticated van der Waals structures [18]. A very active branch of research investigates spatially indirect interlayer excitons in TMD heterobilayers of with great prospects for spin-valley physics and nano-scale Moire potentials [19–25].

In this work we investigate interlayer excitons in homobilayers of MoS₂. Contrary to interlayer excitons in TMD heterobilayers, which are indirect both in real and reciprocal space, we find strong signatures in absorption of the interlayer exciton, about 20 % of the oscillator strength of the intralayer exciton. Our DFT-GW calculations solving the Bethe-Salpeter equation un-

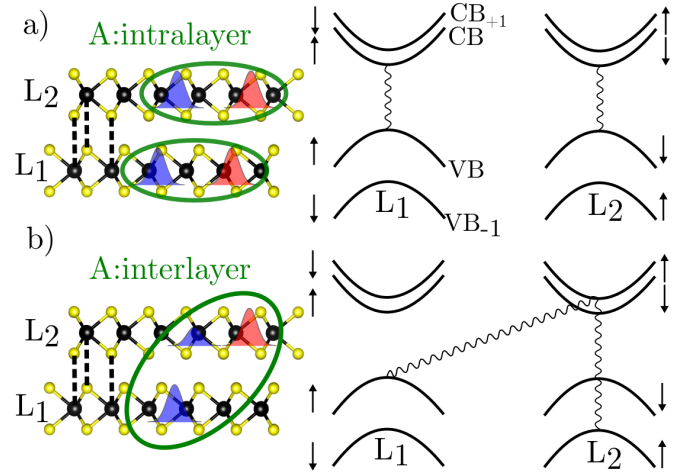


FIG. 1: **Schematics of intralayer and interlayer excitons in MoS₂ homobilayers.** (a) Intralayer excitons consist of an electron (red) and a hole (blue) in the same layer while in b) an electron localized on one layer interacts with a hybridized hole state to form an interlayer exciton. Optical selection rules, represented by wavy lines, for intralayer and interlayer transitions in k -space are also given for K points, respecting spin conservation. For clarity only one interlayer exciton (spin up) is shown, there is also the spin down state with the same energy.

cover a strong, spin allowed interlayer exciton peak about 80 meV above the A:1s transition. We find a 20 % reduction of exciton binding energy of the interlayer exciton compared to the intralayer exciton. Our calculated absorption also predicts an interlayer transition involving the B-valence band located in energy above the B:1s intralayer transition. We compare several bilayer stackings in our calculations of optical absorption spectra [10, 26]. Our experiments on high quality bilayer and

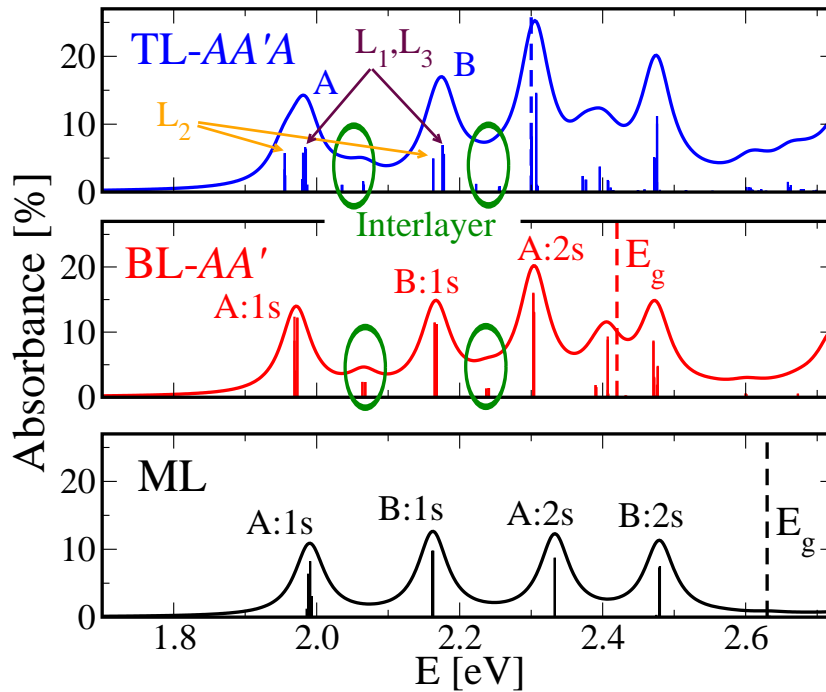


FIG. 2: **Calculated absorption spectra for a single mono-, bi and tri-layer.** Interlayer exciton transitions are marked by green circles. Orange arrows for the TL case indicate intralayer transitions involving only the middle layer (L_2) of the three layers, while the maroon ones stress the L_1, L_3 intralayer transitions. See text and appendix for computational details.

trilayer MoS_2 in hBN show prominent signatures of interlayer excitons up to room temperature in absorption, signalling strong oscillator strength. The clear manifestation of interlayer excitons opens the way for electric field control of the optical transitions based on their out-of-plane electric dipole [12]. Their strong oscillator strength makes this in addition an interesting system for efficient, tunable coupling to optical microcavities and plasmons [27–31]. Our work shows directly the stronger interlayer coupling for the hole states in MoS_2 as compared to much weaker coupling expected for K-excitons in WSe_2 homobilayers due to the larger A-B valence band separation [32, 33].

The paper is organized as follows : First in section we calculate the bandstructure and optical absorption spectra. Then in section we present the corresponding absorption experiments in high quality monolayer, bilayer and trilayer samples. Finally we discuss the comparison between experiment and theory as well as open questions in section . Computational and experimental details can be found in the Appendices and .

BAND STRUCTURE AND ABSORPTION SPECTRA CALCULATIONS

The natural MoS_2 bilayer (BL) stacking is AA', see Fig.3a for atomic stacking representation, corresponding to the $2H$ bulklike symmetry. This is thermodynamically the most stable configuration at the highly accurate Random Phase Approximation level of correlation energy calculations [34]. In our case, when using the DFT-D3 exchange-correlation functional scheme of Grimme *et al* [35], the AB-stacking, prototypical of the $3R$ -structure [26], has the same binding energy within meV accuracy, i.e 117 meV/formula unit. In other words, both monolayers gain 117 meV (per elementary cell) by forming a bilayer as compared to staying at infinite distance. AA-stacking is much less favorable: 82 meV per formula unit. The interlayer distance d_{inter} we find is similar for AA' and AB stacking order, being 6.17 Å, in good agreement with previous studies [34, 36].

In Figure 2, we provide absorption spectra calculated from the imaginary part of the complex dielectric function extracted from GW +BSE procedure see the appendix for more details, for freestanding ML, BL-AA' and trilayer (TL) in $2H$ -like stacking systems, which are the most relevant for samples exfoliated from naturally occurring MoS_2 . So our calculations for the absorbance are based on a precise determination of the bandstruc-

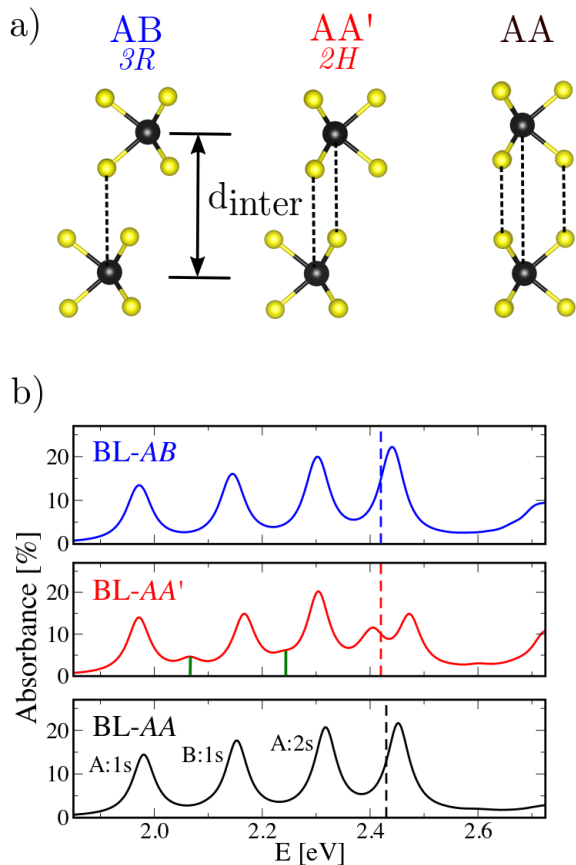


FIG. 3: **Calculated absorption spectra for a bilayer, using three different stackings.** The green lines mark interlayer transitions for AA' stackings.

ture and then including the strong excitonic effects. In order to validate our computational approach and precision, which is of the order of few tens of meV for excitonic peak positions, we perform calculations for monolayer MoS₂ in vacuum and we identify and reproduce the peak positions of the different spectral features as in the work of Qiu *et al.* [37, 38]. Note that the 2s feature oscillator strengths are overestimated due to limited number of k-points used in the response function calculations in the BSE step of the calculations. The monolayer results give us confidence for the bilayer system where comparison with experimental data was so far not possible in detail because of the poor optical quality of the structures. As expected, when the number of layers is increased the fundamental gap E_g at the K-point is decreased: 2.62, 2.43 and 2.30 eV for ML, BL and TL respectively, when the multi-layered systems become globally indirect in the Γ -K direction, as it can be seen in Fig. S1.

In our calculated AA'-BL absorption spectrum we find an additional transition between the A and B intralayer exciton 1s states, 0.09 eV above the A and B peaks, see Fig. 2. This peak consists of four degenerate transitions due to spin-splitting and K-K' equivalence. Consider-

ing only the spin up in K valley transition as proposed in Fig.1b), it has 19 % of the oscillator strength of the corresponding A:1s intralayer transition. Its main contributions come from states corresponding to the valence band spin up: VB of L₁ and VB₋₁ of L₂ partially hybridized, and a well-localized electron lying in the second lowest conduction band (CB₊₁) states of the other layer. Surprising is the high oscillator strength for this spatially indirect transition, not predicted in earlier work on similar systems [12]. Here the hole states delocalized over the bilayer are important, as the transition we call for brevity interlayer has an intralayer contribution, sketched in Fig.1b : the intralayer (L₂) VB₋₁ to CB₊₁ oscillator strength is roughly 18% of the spatially indirect VB to CB₊₁ one. We recall that the symmetry of the first VBs in K are mainly of $d_{x^2-y^2}$ and d_{xy} characters, mixed with $p_{x,y}$ orbitals of S, when the first CBs are made of d_{z^2} orbitals. Interlayer hopping (hybridization) are thus possible in the VBs, helped by the S- p_z orbital contributions in Γ , but remains impossible for electrons in the CBs [10, 26, 39].

Quantitative analysis of the optical transitions in the related system of MoSe₂ bilayers in hBN using the Dirac-Bloch equations also predicts an oscillator strength of 20 % of the interlayer A-exciton compared to the intralayer exciton [15]. In their work the encapsulation in hBN is taken explicitly taken into account, whereas our calculations are performed in vacuum to avoid high computational cost. Our general target was to see what type of new exciton absorption feature emerges as we go from monolayer to bilayer material - the exact energy position of the transition will be sensitive to screening by the dielectric environment [40, 41]. We extract in BL MoS₂ the exciton binding energies for the intralayer excitons of about 0.45 eV compared to 0.36 eV for interlayer excitons. This relative comparison shows strong binding for interlayer excitons with carriers residing in different layers, although the absolute values will be smaller in encapsulated samples in hBN principally due to expected band gap renormalization [41].

For the TL case shown in Fig. 2, several interesting features are observed: the A:1s state is split, with the intralayer exciton of the central layer (L₂) having the largest binding energy and followed in energy by intralayer excitons from the two outside layers (L₁,L₃). In our calculations we also see clear signatures of interlayer excitons in TLs. A set of interlayer transitions is present 0.05 eV above the A peak and again split by 0.03 eV due to the possibility for the carriers to reside either in the central or outside layers. The interlayer exciton oscillator strengths are relatively large as in the bilayer case, around 20% of the intralayer transitions.

Interlayer coupling of VBs and CBs is governed by symmetry and also the spin-orbit splitting between spin-up and spin-down bands, as revealed in very early work in bulk samples [17]. Whereas interlayer coupling for

electrons is suppressed by symmetry also for AA' stacking [10], the interlayer coupling for hole states depends on both symmetry (and more specifically on atomic arrangement between layers) and, if allowed, also on the amplitude of the spin-orbit splitting [10, 26]. In that respect AA' stacking in bilayer MoS₂ provides favorable conditions for the observation of interlayer excitons, as the interlayer coupling of VBs is allowed and the spin-orbit splitting is smaller than in MoSe₂, MoTe₂, WSe₂ and WS₂. So for sake of completeness, we also calculated the absorption spectra for AA and AB stacking (corresponding to $\mathcal{3R}$ symmetry in bulk), for which we observe no signature interlayer exciton transitions as shown in the comparison in Fig.3.

OPTICAL SPECTROSCOPY ON MOS₂ MONO-,BI- AND TRILAYERS IN HBN

Bilayer MoS₂ is a fascinating system with tunable properties, explored in a large spectrum of theoretical work [10, 12, 42–45] and also experiments [36, 46–48]. So far experimental studies of optical properties concentrated on the intralayer exciton. As bilayer MoS₂ has an indirect gap, the technique of choice is absorption spectroscopy, either in transmission or reflection geometry, emission in photoluminescence on the other hand is strongly quenched compared to the monolayer [4, 5]. Further progress was hampered until recently by the very broad optical transition linewidth in MoS₂ based nanostructures of the order of 50 meV. Encapsulation in hexagonal boron nitride (hBN) of MoS₂ monolayers (MLs) has resulted in considerable narrowing of the exciton transition linewidth down to 1 meV [49, 50] and allowed identification of excited exciton states [51]. This gives access to fine features of the exciton spectra and considerably clearer comparison with theory. We fabricated a sample with monolayer steps (ML, BL, TL) encapsulated in hBN, see Appendix for details, so we compare all 3 different thicknesses in identical conditions, see Fig. 4. Atomic force microscopy (AFM) measurements have been performed in tapping mode, before deposition of the top hBN layer. The topography of Fig. 4b shows height steps corresponding to monolayer, bilayer and trilayer MoS₂. The extremely different white light reflectivity spectra in Fig. 4c are so striking, they can be used for thickness identification, as discussed below. As this sample is exfoliated from $2H$ bulk, the bilayer stacking is the thermodynamically most stable AA' configuration, analyzed in detail by DFT in the previous section.

Low temperature differential reflectivity

First we discuss the measurements at low temperature $T=4$ K. We measure differential reflectivity ($R_{\text{ML}} -$

$R_{\text{sub}})/R_{\text{sub}}$, where R_{ML} is the intensity reflection coefficient of the sample with the MoS₂ layer and R_{sub} is the reflection coefficient of the hBN/SiO₂ stack. Please note that the overall shape of the differential reflectivity depends on cavity effects (thin layer interference) given by top/bottom hBN and SiO₂ thickness. This leads to exciton transition lineshape variations in amplitude and sign in the presented spectra, see [51] for a detailed discussion and comparison with transfer matrix simulations.

Monolayer. As for theory, also for experiment the 1ML sample allows us to validate our approach : the spectra are very similar to the exciton states identified for hBN encapsulated MoS₂ in previous work [51], with a clear signature of the A:2s exciton state superimposed on B:1s, where we find a typical A-B exciton separation of 150 meV in energy [39]. Here cavity effects determined by the top and bottom hBN thickness used for encapsulation need to be taken into account to analyze the oscillator strength [51]. The identification of the A:2s and A:3s as excited A-excitons is confirmed by analyzing the diamagnetic shift in magneto-absorption [52] and using photoluminescence excitation experiments [51]. Note that for the monolayer A:1s to A:2s separation we find an energy of about 170 meV. This is less than the 1s to 2s exciton state separation measured for the B-exciton in uncapped monolayer MoS₂ on hBN/SiO₂ of about 225 meV [53]. This follows the general trend of finding lower exciton binding energies in hBN encapsulated samples as compared to non-encapsulated ones, underlining the importance of the dielectric environment for the strength of the Coulomb interaction [40, 54].

Bilayer. The difference between ML and BL absorption is striking : there is an additional transition in Fig. 4c right between A:1s and B:1s. We attribute this transition 70 meV above the A:1s to the interlayer exciton, with both carriers at the K-point but in different layers. The energy position between A:1s and B:1s fits well with the predictions from our DFT calculations, compare with Fig. 2. In the region of the B-exciton we find 2 transitions. In addition to B:1s the second peak could be linked for example to the A:2s [51] or the interlayer exciton involving the B-valence band, that we see in the calculated absorption spectrum.

Trilayer. Finally we investigate a homotrilayer (TL). Here a striking aspect is the observation of not one but two features associated with the main intralayer A-exciton. Here our DFT calculations suggest, see Fig. 2, that the higher exciton binding energy for intralayer excitons in the middle layer (L_2) results in a lower transition energy as compared to the intralayer excitons from the two outer layers (L_1, L_3). The measured splitting between the two transitions is about 20-25 meV. In addition, between the A- and B-intralayer excitons we observe a feature that we can attribute to interlayer excitons, as we compare our experiment in Fig. 4c with the calculation in Fig. 2. Besides a first strong interlayer exciton we also

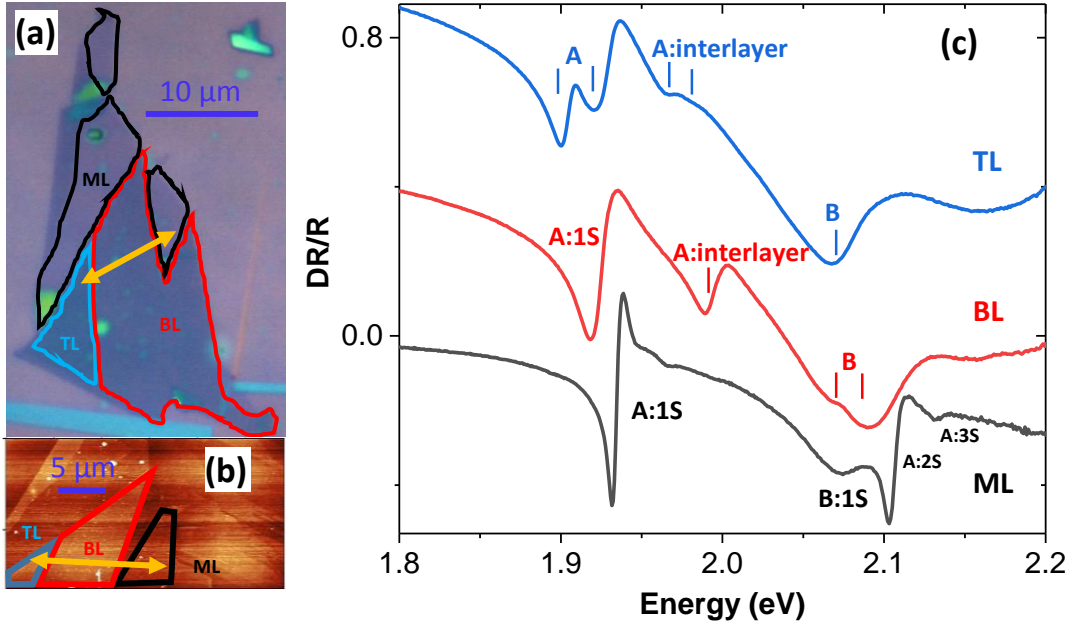


FIG. 4: Monolayer (ML), bilayer (BL) and trilayer (TL) MoS₂ encapsulated in hBN (a) Optical microscope image of the hBN / MoS₂ / hBN heterostructure. (b) AFM measurements confirms atomic steps. (c) Differential reflectivity of the three different thicknesses (ML, BL and TL) at a sample temperature of T=4 K, spectra offset for clarity.

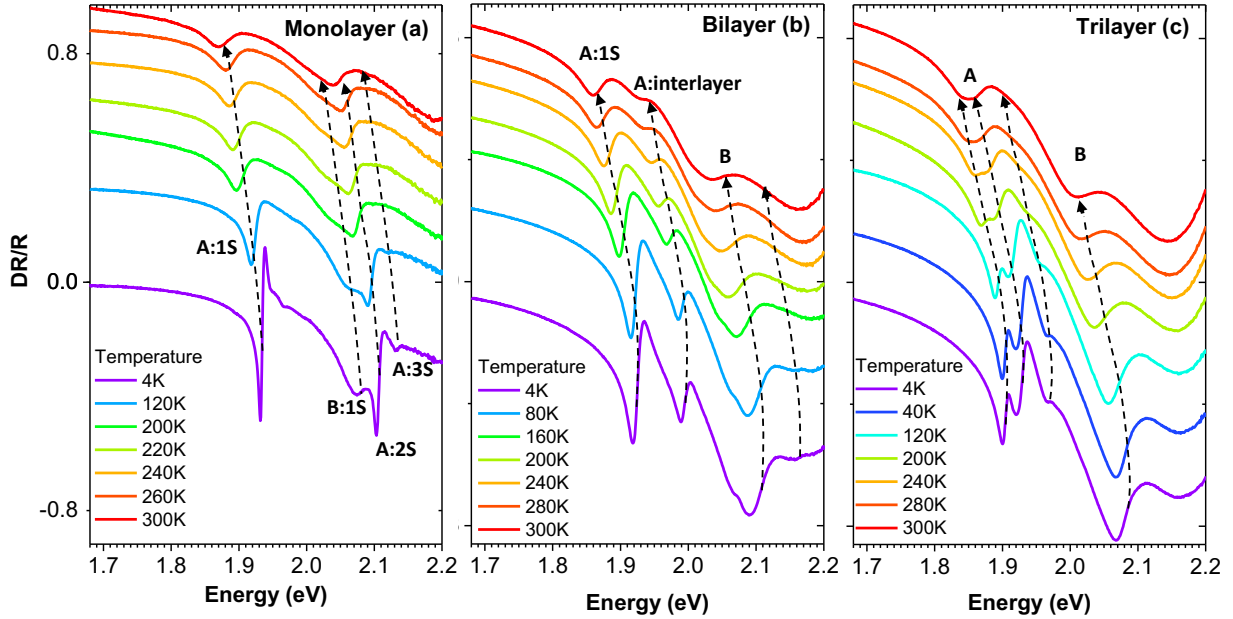


FIG. 5: **Optical spectroscopy results:** Temperature dependent differential reflectivity spectra for monolayer (a), bilayer (b) and trilayer (c) MoS₂ encapsulated in hBN.

observe a second feature about 15 meV above in energy. From our DFT calculations for the interlayer exciton different energies are expected for carriers residing in the inner or outer layers, similar to the splitting observed in the intralayer exciton case.

Both homobilayer and trilayers are indirect semicon-

ductors. The optical transitions involving excitons direct in momentum space with carriers from the K-points can be broadened compared to the ML case due to relaxation towards the lower lying indirect bandgap.

Temperature evolution of absorption from 4 K to room temperature

In Fig. 5 we analyze the temperature evolution of the differential reflectivity spectra. The evolution of the ML spectrum up to room temperature shows a standard shift of the A:1s transition with temperature. At 300 K at first glance two strong transitions are visible, separated by 170 meV. The B:1s absorption is very broad and its energy cannot be fitted precisely. Surprisingly, the most pronounced feature at higher energy is not the B:1s but the A:2s state. In general to observe excited exciton states also at room temperature is consistent with the high binding energy of these intralayer excitons in hBN encapsulated MoS₂ of about 220 meV [51].

Remarkably, for the bilayer in Fig. 5b the intralayer but also the interlayer transition are still observable at room temperature, again consistent with a high exciton binding energy, as indicated by our *ab initio* results. For the trilayer, the double feature for the intralayer A-exciton is visible at all temperatures. The main interlayer exciton is still discernible at 240 K.

DISCUSSION

For simplicity, in our theory and experiment we concentrate on optical transitions with large oscillator strength, so in our optical absorption spectra we have no clear signature of possible optical transitions indirect in k-space, for example, that involve carriers from the Γ -point [55, 56]. In this work we exclusively discuss transitions involving carriers in different layers and bands, but all at the K-point. The band structure of TMD bilayers is rather complex at the K-point, with spin-split conduction and valence bands [10, 57, 58]. Already in a single particle picture this gives rise to several optical transitions. In optical spectroscopy experiments we work with excitons not band to band transitions, so all energy scales are renormalized by the Coulomb interaction, the direct and exchange terms.

We now try to analyze why the interlayer and intralayer A-excitons have different transition energies, similar arguments hold for the B-excitons. In the bilayer absorption measurements in Figs. 4c and 5b and also calculations in Fig. 2 we observe the intralayer exciton transition about $\Delta_{\text{exp}} = 70$ meV lower in energy than the interlayer exciton. Several effects can contribute to this difference :

(i) Difference in intralayer (calculated 0.45 eV) and interlayer exciton binding energy (0.36 eV). Although the calculations are for structures in vacuum and our sample is encapsulated in hBN, we see this difference is significant and will provide an important contribution to Δ_{exp} . The physical origin of the difference in binding energies can come from the different spatial extension of the exci-

ton in the intra- and interlayer configuration. The effective mass for spin-up and spin-down conduction and valence bands that we can extract from our band structure calculations is another source for differences in the binding energies of different exciton species [39]. For the A-interlayer exciton the difference in mass of the two lowest lying conduction bands is relevant, and we find $0.47 m_0$ for CB₊₁ and $0.42 m_0$ for CB, respectively, where m_0 is the free electron mass. Though significant, our calculations show this mass difference remains a smaller contribution compared to the exciton spatial extension change between the two configurations.

(ii) Due to spin-conservation in optical dipole transitions, the interlayer excitons is formed with an electron in the second lowest, not lowest conduction band, see Fig. 1b. The conduction band spin splitting is estimated to be in the meV range [57, 58], we find 13 meV in our calculations, see Fig. S1, in very good agreement with a recent experimental measurement [59]. So this conduction band spin splitting can contribute to Δ_{exp} , but is not the dominating term.

(iii) The exchange terms of the Coulomb interaction are also important and for the case of MoS₂ might reverse the order in energy of the spin-allowed and spin forbidden transitions [60, 61].

In a very recent preprint interlayer excitons in MoS₂ [62] are discussed in detail for bilayer and trilayers using k.p theory and comparing with magneto-optics. Although the theoretical approach is very different from our *ab-initio* calculations, both approaches agree on the existence and importance of interlayer K-point excitons. Predicting the exact energy positions is still challenging due to the uncertainties in amplitude and sign of the conduction band spin splitting [63], the Coulomb exchange terms and also the effective masses [59], see [62] for a complementary analysis.

In conclusion, interlayer excitons with high oscillator strength are found in post-DFT calculations and optical absorption measurements on MoS₂ homobilayers and trilayers. Their optical signatures are visible up to room temperature. The interlayer excitons involve an electron in one layer and a hole delocalized over both layers. This combines in principle large oscillator strength with a large static dipole moment, which is a desirable configuration for coupling quantum tunneling with cavity photons, previously reported at cryogenic temperatures in III-V semiconductor nano-structures [64].

We thank Alexandre Pierrot and Benjamin Lassagne for technical assistance with AFM measurements. We thank Kristian Thygesen, Clement Faugeras, Misha Glazov and Atac Imamoglu for stimulating discussions. We acknowledge funding from ANR 2D-vdW-Spin, ANR VallEx, Labex NEXT projects VWspin and MILO, ITN Spin-NANO Marie Sklodowska-Curie grant agreement No 676108 and ITN 4PHOTON Nr. 721394. X.M. also acknowledges the Institut Universitaire de France.

Growth of hexagonal boron nitride crystals was supported by the Elemental Strategy Initiative conducted by the MEXT, Japan and the CREST (JPMJCR15F3), JST. Finally, I. C. Gerber thanks the CALMIP initiative for the generous allocation of computational times, through the project p0812, as well as the GENCI-CINES and GENCI-IDRIS for the grant A004096649.

Computational Details

The atomic structures, the quasi-particle band structures and optical spectra are obtained from DFT calculations using the VASP package [65, 66]. It uses the plane-augmented wave scheme [67, 68] to treat core electrons. Perdew-Burke-Ernzerhof (PBE) functional [69] is used as an approximation of the exchange-correlation electronic term, to build the starting wave-function for GW calculations. During geometry's optimization step of all the hetero-structures, performed at the PBE-D3 level [35], all the atoms were allowed to relax with a force convergence criterion below $0.005 \text{ eV}/\text{\AA}$, in order to include van der Waals interaction between layers. The optimized lattice parameter of MoS_2 , obtained at the PBE level, used for all the calculations is 3.22 \AA . A grid of $15 \times 15 \times 1$ k-points has been used, in conjunction with a vacuum height of 21.9 \AA , for all the calculation cells, to take benefit of error's cancellation in the band gap estimates [70], and to provide absorption spectra in good agreement with experiments [71, 72]. An energy cutoff of 400 eV and a gaussian smearing of 0.05 eV width have been chosen for partial occupancies, when a tight electronic minimization tolerance of 10^{-8} eV is set to determine with a good precision the corresponding derivative of the orbitals with respect to k needed in quasi-particle band structure calculations. Spin-Orbit Coupling (SOC) was also included non-self-consistently to determine eigenvalues and wave functions as input for the full-frequency-dependent GW calculations [73] performed at the G_3W_0 level [60]. The total number of states included in the GW procedure is set to 1280, in conjunction with an energy cutoff of 100 eV for the response function, after a careful check of the direct band gap convergence (smaller than 0.1 eV as a function of k-points sampling). Band structures have been obtained after a Wannier interpolation procedure performed by the WANNIER90 program [74]. All optical excitonic transitions have been calculated by solving the Bethe-Salpeter Equation [75, 76], using the twelve highest valence bands and the sixteen lowest conduction bands to obtain eigenvalues and oscillator strengths on all systems. From these calculations, we report the absorbance values by using the imaginary part of the complex dielectric function.

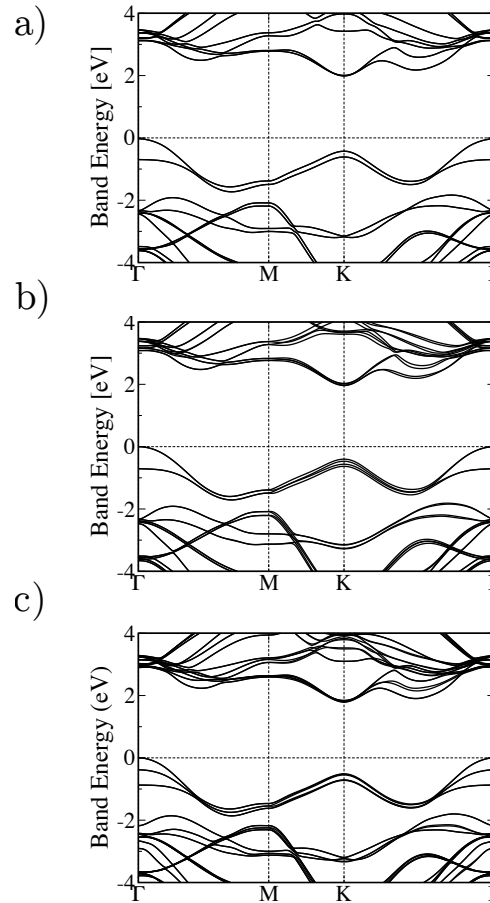


FIG. S1: **Quasiparticle band structures** at the G_3W_0 level in a) AA' BL, b) AB BL and c) AA'A TL stacking.

Experimental Methods

The samples are fabricated by mechanical exfoliation of bulk MoS_2 (commercially available from 2D bulk semiconductors) and very high quality hBN crystals on 83-nm SiO_2 [77] on a Si substrate. The experiments are carried out in a confocal microscope built in a vibration free, closed cycle cryostat with variable temperature. The excitation/detection spot diameter is $\sim 1 \mu\text{m}$. Reflectivity measurements were performed with a power-stabilized white halogen lamp for sample temperatures $T = 4 - 300 \text{ K}$. The reflectivity signal is dispersed in a spectrometer and detected with a Si-CCD camera [51].

* Electronic address: igerber@insa-toulouse.fr

† Electronic address: urbaszek@insa-toulouse.fr

- [1] K. S. Novoselov, A. Mishchenko, A. Carvalho, and A. H. Castro Neto, *Science* **353** (2016).
- [2] A. K. Geim and I. V. Grigorieva, *Nature* **499**, 419 (2013).
- [3] Y. Zhang, T.-T. Tang, C. Girit, Z. Hao, M. C. Martin,

- A. Zettl, M. F. Crommie, Y. R. Shen, and F. Wang, *Nature* **459**, 820 (2009).
- [4] K. F. Mak, C. Lee, J. Hone, J. Shan, and T. F. Heinz, *Phys. Rev. Lett.* **105**, 136805 (2010).
- [5] A. Splendiani, L. Sun, Y. Zhang, T. Li, J. Kim, C.-Y. Chim, G. Galli, and F. Wang, *Nano Letters* **10**, 1271 (2010).
- [6] G. Bastard, E. Mendez, L. Chang, and L. Esaki, *Physical Review B* **26**, 1974 (1982).
- [7] G. Wang, A. Chernikov, M. M. Glazov, T. F. Heinz, X. Marie, T. Amand, and B. Urbaszek, *Rev. Mod. Phys.* **90**, 021001 (2018).
- [8] K. He, N. Kumar, L. Zhao, Z. Wang, K. F. Mak, H. Zhao, and J. Shan, *Phys. Rev. Lett.* **113**, 026803 (2014).
- [9] A. Chernikov, T. C. Berkelbach, H. M. Hill, A. Rigosi, Y. Li, O. B. Aslan, D. R. Reichman, M. S. Hybertsen, and T. F. Heinz, *Phys. Rev. Lett.* **113**, 076802 (2014).
- [10] Z. Gong, G.-B. Liu, H. Yu, D. Xiao, X. Cui, X. Xu, and W. Yao, *Nature communications* **4**, 2053 (2013).
- [11] J. Kang, S. Tongay, J. Zhou, J. Li, and J. Wu, *Applied Physics Letters* **102**, 012111 (2013).
- [12] T. Deilmann and K. S. Thygesen, *Nano letters* **18**, 2984 (2018).
- [13] X. Hong, J. Kim, S.-F. Shi, Y. Zhang, C. Jin, Y. Sun, S. Tongay, J. Wu, Y. Zhang, and F. Wang, *Nature nanotechnology* **9**, 682 (2014).
- [14] M. R. Molas, K. Nogajewski, A. O. Slobodeniuk, J. Binder, M. Bartos, and M. Potemski, *Nanoscale* **9**, 13128 (2017).
- [15] J. Horng, T. Stroucken, L. Zhang, E. Y. Paik, H. Deng, and S. W. Koch, *Phys. Rev. B* **97**, 241404 (2018).
- [16] A. Arora, M. Drüppel, R. Schmidt, T. Deilmann, R. Schneider, M. R. Molas, P. Marauhn, S. M. de Vasconcelos, M. Potemski, M. Rohlfling, et al., *Nature communications* **8**, 639 (2017).
- [17] A. R. Beal and W. Y. Liang, *Journal of Physics C: Solid State Physics* **9**, 2459 (1976).
- [18] E. Calman, M. Fogler, L. Butov, S. Hu, A. Mishchenko, and A. Geim, *Nature communications* **9**, 1895 (2018).
- [19] P. Rivera, K. L. Seyler, H. Yu, J. R. Schaibley, J. Yan, D. G. Mandrus, W. Yao, and X. Xu, *Science* **351**, 688 (2016).
- [20] P. Nagler, M. V. Ballottin, A. A. Mitroglu, F. Mooshammer, N. Paradiso, C. Strunk, R. Huber, A. Chernikov, P. C. Christianen, C. Schüller, et al., *Nature Communications* **8**, 1551 (2017).
- [21] K. Tran, G. Moody, F. Wu, X. Lu, J. Choi, A. Singh, J. Embley, A. Zepeda, M. Campbell, K. Kim, et al., *ArXiv e-prints* (2018), 1807.03771.
- [22] K. L. Seyler, P. Rivera, H. Yu, N. P. Wilson, E. L. Ray, D. Mandrus, J. Yan, W. Yao, and X. Xu, *ArXiv e-prints* (2018), 1809.04562.
- [23] C. Zhang, C.-P. Chuu, X. Ren, M.-Y. Li, L.-J. Li, C. Jin, M.-Y. Chou, and C.-K. Shih, *Science advances* **3**, e1601459 (2017).
- [24] H. Yu, G.-B. Liu, J. Tang, X. Xu, and W. Yao, *Science advances* **3**, e1701696 (2017).
- [25] N. Zhang, A. Surrente, M. Baranowski, D. K. Maude, P. Gant, A. Castellanos-Gomez, and P. Plochocka, *Nano Letters* **ASAP**, null (2018).
- [26] R. Akashi, M. Ochi, S. Bordács, R. Suzuki, Y. Tokura, Y. Iwasa, and R. Arita, *Phys. Rev. Applied* **4**, 014002 (2015).
- [27] M. M. Fogler, L. V. Butov, and K. S. Novoselov, *Nat Commun* **5**, 10.1038/ncomms5555 (2014).
- [28] C. Schneider, M. M. Glazov, T. Korn, S. Hfling, and B. Urbaszek, *Nature Comms.* **3**, 2695 (2018).
- [29] T. Low, A. Chaves, J. D. Caldwell, A. Kumar, N. X. Fang, P. Avouris, T. F. Heinz, F. Guinea, L. Martin-Moreno, and F. Koppens, *Nature materials* **16**, 182 (2017).
- [30] X. Liu, T. Galfsky, Z. Sun, F. Xia, E.-c. Lin, Y.-H. Lee, S. Kéna-Cohen, and V. M. Menon, *Nature Photonics* **9**, 30 (2015).
- [31] S. Dufferwiel, S. Schwarz, F. Withers, A. Trichet, F. Li, M. Sich, O. Del Pozo-Zamudio, C. Clark, A. Nalitov, D. Solnyshkov, et al., *Nature communications* **6**, 8579 (2015).
- [32] J. Lindlau, M. Selig, A. Neumann, L. Colombier, J. Forste, V. Funk, M. Forg, J. Kim, G. Berghuser, T. Taniguchi, et al., *Nature communications* **9**, 2586 (2018).
- [33] Z. Wang, Y.-H. Chiu, K. Honz, K. F. Mak, and J. Shan, *Nano letters* **18**, 137 (2017).
- [34] J. He, K. Hummer, and C. Franchini, *Physical Review B* **89**, 075409 (2014).
- [35] S. Grimme, J. Antony, S. Ehrlich, and H. Krieg, *J. Chem. Phys.* **132**, 154104 (2010).
- [36] K. Liu, L. Zhang, T. Cao, C. Jin, D. Qiu, Q. Zhou, A. Zettl, P. Yang, S. G. Louie, and F. Wang, *Nature Communications* **5**, 4966 (2014).
- [37] D. Y. Qiu, F. H. da Jornada, and S. G. Louie, *Phys. Rev. Lett.* **111**, 216805 (2013).
- [38] D. Y. Qiu, T. Cao, and S. G. Louie, *Phys. Rev. Lett.* **115**, 176801 (2015).
- [39] A. Kormányos, G. Burkard, M. Gmitra, J. Fabian, V. Zolyomi, N. D. Drummond, and V. Fal'ko, *2D Materials* **2**, 022001 (2015).
- [40] A. V. Stier, N. P. Wilson, G. Clark, X. Xu, and S. A. Crooker, *Nano Letters* **16**, 7054 (2016).
- [41] I. C. Gerber and X. Marie, *ArXiv e-prints* (2018), 1810.02130.
- [42] T. Cheiwchanchamnangij and W. R. L. Lambrecht, *Phys. Rev. B* **85**, 205302 (2012).
- [43] S. Bhattacharyya and A. K. Singh, *Physical Review B* **86**, 075454 (2012).
- [44] Q. Liu, L. Li, Y. Li, Z. Gao, Z. Chen, and J. Lu, *The Journal of Physical Chemistry C* **116**, 21556 (2012).
- [45] A. Kormányos, V. Zolyomi, V. I. Fal'ko, and G. Burkard, *Phys. Rev. B* **98**, 035408 (2018).
- [46] H. Wang, L. Yu, Y.-H. Lee, Y. Shi, A. Hsu, M. L. Chin, L.-J. Li, M. Dubey, J. Kong, and T. Palacios, *Nano letters* **12**, 4674 (2012).
- [47] S. Wu, J. S. Ross, G.-B. Liu, G. Aivazian, A. Jones, Z. Fei, W. Zhu, D. Xiao, W. Yao, D. Cobden, et al., *Nature Physics* **9**, 149 (2013).
- [48] T. Jiang, H. Liu, D. Huang, S. Zhang, Y. Li, X. Gong, Y.-R. Shen, W.-T. Liu, and S. Wu, *Nature nanotechnology* **9**, 825 (2014).
- [49] F. Cadiz, E. Courtade, C. Robert, G. Wang, Y. Shen, H. Cai, T. Taniguchi, K. Watanabe, H. Carrere, D. Lagarde, et al., *Phys. Rev. X* **7**, 021026 (2017).
- [50] O. A. Ajayi, J. V. Ardelean, G. D. Shepard, J. Wang, A. Antony, T. Taniguchi, K. Watanabe, T. F. Heinz, S. Strauf, X. Zhu, et al., *2D Materials* **4**, 031011 (2017).
- [51] C. Robert, M. A. Semina, F. Cadiz, M. Manca, E. Courtade, T. Taniguchi, K. Watanabe, H. Cai, S. Tongay, B. Lussagne, et al., *Phys. Rev. Materials* **2**, 011001 (2018).

- (2018).
- [52] S. Crooker, Private communication (2018).
- [53] H. M. Hill, A. F. Rigosi, C. Roquelet, A. Chernikov, T. C. Berkelbach, D. R. Reichman, M. S. Hybertsen, L. E. Brus, and T. F. Heinz, *Nano letters* **15**, 2992 (2015).
- [54] A. Raja, A. Chaves, J. Yu, G. Arefe, H. M. Hill, A. F. Rigosi, T. C. Berkelbach, P. Nagler, C. Schüller, T. Korn, et al., *Nature communications* **8**, 15251 (2017).
- [55] W. Zhao, R. M. Ribeiro, M. Toh, A. Carvalho, C. Kloc, A. H. Castro Neto, and G. Eda, *Nano Letters* **13**, 5627 (2013).
- [56] A. Kormányos, V. Zólyomi, N. D. Drummond, P. Rakyta, G. Burkard, and V. I. Fal'ko, *Phys. Rev. B* **88**, 045416 (2013).
- [57] K. Kośmider, J. W. González, and J. Fernández-Rossier, *Phys. Rev. B* **88**, 245436 (2013).
- [58] G.-B. Liu, W.-Y. Shan, Y. Yao, W. Yao, and D. Xiao, *Phys. Rev. B* **88**, 085433 (2013).
- [59] R. Pisoni, A. Kormányos, M. Brooks, Z. Lei, P. Back, M. Eich, H. Overweg, Y. Lee, P. Rickhaus, K. Watanabe, et al., *ArXiv e-prints* (2018), 1806.06402.
- [60] J. P. Echeverry, B. Urbaszek, T. Amand, X. Marie, and I. C. Gerber, *Phys. Rev. B* **93**, 121107 (2016).
- [61] X.-X. Zhang, T. Cao, Z. Lu, Y.-C. Lin, F. Zhang, Y. Wang, Z. Li, J. C. Hone, J. A. Robinson, D. Smirnov, et al., *Nature nanotechnology* **12**, 883 (2017).
- [62] A. O. Slobodeniuk, L. Bala, M. Koperski, M. R. Molas, P. Kossacki, K. Nogajewski, M. Bartos, K. Watanabe, T. Taniguchi, C. Faugeras, et al., *ArXiv e-prints* (2018), 1810.00623.
- [63] M. Molas, C. Faugeras, A. Slobodeniuk, K. Nogajewski, M. Bartos, D. Basko, and M. Potemski, *2D Materials* **4**, 021003 (2017).
- [64] P. Cristofolini, G. Christmann, S. I. Tsintzos, G. Deligeorgis, G. Konstantinidis, Z. Hatzopoulos, P. G. Savvidis, and J. J. Baumberg, *Science* **336**, 704 (2012).
- [65] G. Kresse and J. Hafner, *Phys. Rev. B* **47**, 558 (1993).
- [66] G. Kresse and J. Furthmüller, *Phys. Rev. B* **54**, 11169 (1996).
- [67] P. E. Blöchl, *Phys. Rev. B* **50**, 17953 (1994).
- [68] G. Kresse and D. Joubert, *Phys. Rev. B* **59**, 1758 (1999).
- [69] J. P. Perdew, K. Burke, and M. Ernzerhof, *Phys. Rev. Lett.* **77**, 3865 (1996).
- [70] F. Hüser, T. Olsen, and K. S. Thygesen, *Phys. Rev. B* **88**, 245309 (2013).
- [71] A. R. Klots, A. K. M. Newaz, B. Wang, D. Prasai, H. Krzyzanowska, D. Caudel, N. J. Ghimire, J. Yan, B. L. Ivanov, K. A. Velizhanin, et al., *Scientific Reports* **4**, 6608 (2014).
- [72] A. Molina-Sánchez, D. Sangalli, K. Hummer, A. Marini, and L. Wirtz, *Physical Review B* **88**, 045412 (2013).
- [73] M. Shishkin and G. Kresse, *Phys. Rev. B* **74**, 035101 (2006).
- [74] A. A. Mostofi, J. R. Yates, Y.-S. Lee, I. Souza, D. Vanderbilt, and N. Marzari, *Computer Physics Communications* **178**, 685 (2008).
- [75] W. Hanke and L. J. Sham, *Phys. Rev. Lett.* **43**, 387 (1979).
- [76] M. Rohlfing and S. G. Louie, *Phys. Rev. Lett.* **81**, 2312 (1998).
- [77] T. Taniguchi and K. Watanabe, *Journal of Crystal Growth* **303**, 525 (2007).